*Second International Conference on CFD in the Minerals and Process Industries*
*CSIRO, Melbourne, Australia*
*6-8 December 1999*

# STABILIZATION OF UNSTEADY TURBULENT FLOW IN THE MOLD REGION OF A WIDE SLAB CASTER BY SUBMERGED ENTRY NOZZLE DESIGN OPTIMIZATION WITH CFD

**Markus BRUMMAYER[1], Philipp GITTLER[1], Josef WATZINGER[2]**

[1]Department of Fluid Dynamics and Heat Transfer, J. K. University Linz, 4040 Linz, AUSTRIA
[2]Thin Slab Casting and Direct Rolling – VOEST-ALPINE Industieanlagenbau GmbH, 4031 Linz, AUSTRIA

## ABSTRACT

Plate mill casters producing slabs of medium thickness and large width at high steel throughput up to 4 tons per minute require special casting technologies and can be termed as wide slab casters.

Comprehensive metallurgical investigations concerning slab quality defects very clearly indicate the strong influence of the mold flow conditions on slab quality (Gotthelf et al., 1998; Heaslip and Schade, 1999).

Flow patterns in the mold region of commercial slab casters at conventional casting widths are well known. Also unsteady flow patterns, specially at wide slab formats, with definite oscillating time periods have been observed by several investigators at water model trials (Gebhard et al., 1993; Honeyands and Herbertson, 1994).

Unsteady turbulent three-dimensional CFD simulations are presented to analyse the influence of the submerged entry nozzle (SEN) geometry on steel velocities and temperature distribution inside the solid shell in the mold region. The numerical model was fine tuned and results were verified by water model trials and by observations.

The main goal of the following numerical studies is to stabilize the unsteady mold flow by optimizing the SEN design.

## NOMENCLATURE

| | |
|---|---|
| $g$ | gravitational acceleration |
| $\Delta h$ | local wave height |
| $\Delta h_{max}$ | maximum wave height |
| $k$ | turbulent kinetic energy |
| $m_j'$ | local mass fraction of species $j'$ |
| $Sc_t$ | turbulent Schmidt number |
| $T_{liq}$ | steel liquidus temperature |
| $T_{ab}$ | temperature above $T_{liq}$ |
| $T_{ab,max}$ | max. temperature above $T_{liq}$ ($T_{ab,max}$ = 40 K) |
| $T_{top}$ | area averaged $T_{ab}$ at free surface |
| $T_0$ | casting temperature at SEN inlet |
| $t$ | simulation time |
| $u_i$ | velocity component in direction $i$ |
| $u_\tau$ | wall friction velocity |
| $v$ | velocity magnitude |
| $v_{top}$ | area averaged velocity magnitude at free surface |
| $W$ | coordinate in slab width direction |
| $W_{max}$ | half slab mold width |
| $x_i$ | $i^{th}$ coordinate direction |
| $y$ | normal distance from the wall to the adjacent cell centers |
| $y^+$ | scaled wall distance |
| $\varepsilon$ | turbulent dissipation rate |
| $\rho$ | density |
| $\rho_j'$ | density of species $j'$ |
| $\mu$ | molecular viscosity |
| $\mu_t$ | turbulent viscosity |

## INTRODUCTION

Flow pattern of slab casters at conventional casting widths up to 2 m have been intensively studied with CFD tools and water models during the last years. In this study the SEN`s used for commercial casters at moderate widths have been tested for wide slab casters. Significant differences in flow pattern and in the amount of characteristic parameters like wave heights and meniscus temperatures have been documented as results of numerical simulations with the commercial CFD code Fluent. However, numerical studies indicate three completely different flow patterns (single roll, double roll, oscillating).

Turbulent flow structures were modeled with Standard k-ε and RNG k-ε turbulence models. Special attention was given to wall friction effects and SEN outlet port flow conditions which were validated by adaptive mesh refinement.

The free surface was modeled as a frictionless wall. With the calculated pressure distribution at this boundary condition the corresponding local wave height and shape can be predicted.

To clarify the flow behavior in the water model trials colored fluid (ink) was injected through the SEN. This visualization of the flow in the mold region was also simulated with a Species Transport Model.

## MODEL FORMULATION

### Governing Equation

Time-dependent 3-D flow of molten steel inside the solid shell in the mold region of a slab caster can be mathematically described by the Reynolds-averaged mass, momentum and energy conservation equations for an incompressible single-phase Newtonian fluid. This set of nonlinear partial equations is well known and not specified here (Schlichting and Gersten, 1997).

### Modeling Turbulent Structures

The Reynolds number based on the nozzle bore diameter is in clearly turbulent regions of $10^5$.

The two-equation Standard k-ε model of Launder and Spalding (1972) and the RNG (renormalization group theory) k-ε model of Yakhot and Orszag (1992) were chosen to close the system of equations.

The ε transport equation of the RNG model includes an additional term which makes this model more responsive to e.g. streamline curvature than the Standard k-ε model. There are no differences in the computation procedure of the turbulent viscosity for high-Reynolds-number mold flows. The empirically determined numerical values of the model constant used in the turbulent viscosity equation are also quite similar.

#### Species Transport Model

To validate the behavior of steel flow in the mold region of the caster a numerical ink experiment was carried out. Convection and turbulent diffusion are the only transport mechanisms in this simulation.
Modeling species transport without chemical reactions and laminar mass diffusion the convection/diffusion equation is simplified to the following form (Fluent Inc., 1998):

$$\frac{\partial}{\partial t}\left(\rho\, m_j'\right)+\frac{\partial}{\partial x_i}\left(\rho\, u_i m_j'\right)=\frac{\partial}{\partial x_i}\left(\frac{\mu_t}{Sc_t}\frac{\partial m_j'}{\partial x_i}\right) \qquad (1)$$

Here $m_j'$ is the local mass fraction of species $j'$, $\mu_t$ is the turbulent viscosity and $Sc_t$ the turbulent Schmidt number.
Both species have the same density

$$\rho_1' = \rho_2' = \rho \qquad (2)$$

where $\rho_1'$ is the density of colored and $\rho_2'$ the density of clear fluid.

## CALCULATION PROCEDURE

#### Unsteady turbulent velocity field

Starting from an initialized zero velocity field the unsteady numerical calculations were carried out with a segregated solution algorithm. Time-dependent terms in the governing equations were discretized by an implicit first order accurate scheme. A converged solution could be attained for a time step of 0.025 s in about 25 iterations. In some cases simulation times up to 800 s were necessary to give correct flow predictions. Validation calculations showed that both turbulence models predict similar turbulent flow behavior while the RNG k-ε turbulence model is by 10 % more CPU time consuming.

#### Temperature field

The energy equation is uncoupled from the other field equations because fluid properties are assumed to be constant.

## GEOMETRY AND BOUNDARY CONDITIONS

#### Geometry and grid generation

The simulated caster length of the straight mold is 4 m and the slab mold thickness is 157 mm for all CFD models. Calculation domains for different nozzle designs at submergence depths in the range of 100 to 225 mm and at mold widths from 2 to 3 m have been modeled. Up to 190.000 finite volume cells of tetraeder shape were used to discretizice the 3-D calculation domain.

#### Simplified boundary conditions for time-dependent simulations

##### *Inlet*

Superheated liquid steel is injected by a SEN in the upper mold region. At the inlet nozzle plane the static pressure and the turbulence parameters $k$ and $\varepsilon$ are fixed. The temperature across the inlet plane is set to casting temperature of $T_0$ = 1833 K ($T_{ab} = T_{ab,max}$ = 40 K).

##### *Outlet*

The water model flow is induced by pumps arranged at the bottom of the model supplying a mass flow which is necessary for adequate casting conditions. The same boundary condition is used in the CFD simulation. Across this bottom outlet the velocity component in casting direction is set to casting speed (1.0 to 1.4 m/min).

##### *Mold wall*

To avoid additional computational difficulties the solidification of liquid steel and the generation of latent heat have not been considered. Here the narrow and wide side of the mold wall present the outer limit of the mushy zone, where the constant liquidus temperature of $T_{liq}$ = 1793 K is specified. Standard wall functions of Launder and Spalding (1974) were used to bridge the viscosity-affected region and to save computational resources. The solidificated shell is moved with casting speed.

##### *Symmetry*

Limiting the calculation mesh to a practical size only one quarter of the whole SEN/mold arrangement was modeled. The simulation of the unsteady behavior of the liquid steel inside the solid shell with this model was verified by numerical simulations and water model trials.

##### *Top surface – meniscus*

The top surface is treated like a frictionless wall where heat losses through flux powder layer were taken into account.

#### Boundary conditions for the Species Transport Model

At the inlet boundary condition an additional parameter for the mass fraction of colored species $m_1'$ appears for the unsteady species transport simulation. The value of $m_1'$ is set to one for 1.5 s at the SEN inlet.

## VALIDATIONS OF THE CFD MODEL

#### Wall friction effects and $y^+$ adaption

Due to the very wide but thin mold format the friction effects between the inner side of the shell and the liquid steel plays an important role. In particular the out-coming side port jets have a long way between the parallel broad plates to reach the narrow side of the mold.
As mentioned above for turbulent flows the standard wall functions were used to gap the viscosity-affected near wall region. These functions work well if the scaled wall distance

$$y^+ = \frac{\rho\, u_\tau\, y}{\mu} \qquad (3)$$

is in the range of 30 to 200. In these simulations $y^+$ reaches a maximum value of 310.

Therefore adaptive grid refinement was performed (Fig. 1) until $y^+$ attained the proposed range. During this operation the grid size increased from 95.000 to 190.000 cells.

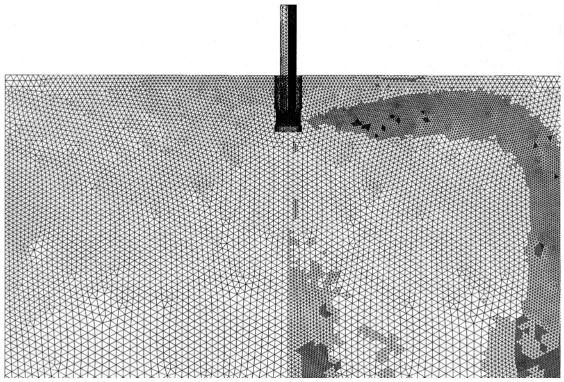

**Figure 1:** Near wall mesh before (left) and after (right) $y^+$ adaption

The unsteady behavior of the side port jet is documented by the time-dependent average velocity magnitude at the top surface of the liquid steel pool $v_{top}$.
As shown in Fig.2 the time-dependent structures of the flow pattern in the upper mold region are similar for both grids and a sufficient number of cells have been used in the slab thickness direction of the coarser grid.

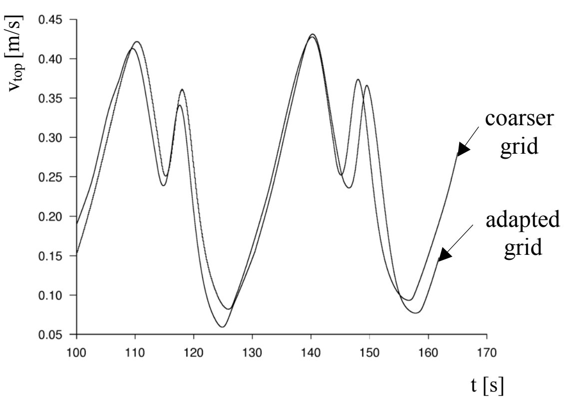


**Figure 2:** Comparison of $v_{top}$ with and without grid adaption

#### Validation of the symmetry boundary conditions at the center plane parallel to the narrow mold side

Due to double symmetry of the physical SEN/mold arrangement it was only necessary to model a quarter of the physical domain. But does this model restriction eliminate important physical phenomena?
To answer this question the grid of the quarter domain was mirrored at the symmetry of the narrow side of the mold. One big symmetry plane which divides in the slab thickness remained. The unsteady simulation was performed in the same manner as for the quarter domain. No significant differences compared to the restricted quarter domain model concerning the characteristical parameters like the time period of side port jet oscillations or the impingement point position were observed. Numerical simulations of the whole SEN/mold configuration confirmed the nature of oscillations calculated with the quarter domain model.

#### Calculation of the wave height of the top surface

Principally the top surface of the mold was assumed to be flat for the time-dependent turbulent calculations. However, the pressure distribution at the surface can be used to predict the expected shape of the wave. The estimated wave height is balanced with the local pressure

$$p = \rho \, g \, \Delta h \qquad (4)$$

where $g$ is the accelerating due to gravitation and $\Delta h$ is the local wave height.

### RESULTS AND DISCUSSION

#### Verification of the flow patterns observed at water trials with numerical ink experiments

The characteristic parameters which are used to describe the flow patterns of liquid steel or water are defined in Fig. 3.

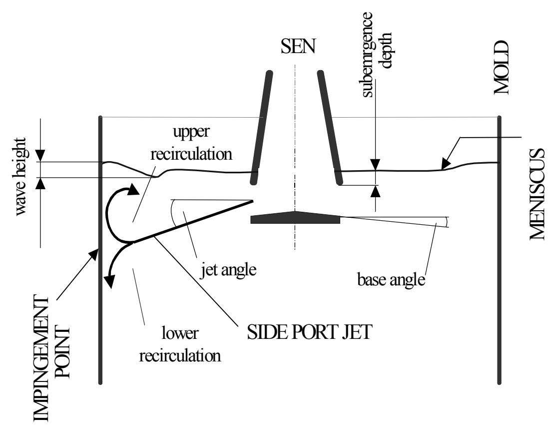


**Figure 3:** Sketch of mold flow pattern and definitions

To visualize the flow structures inside the water model ink colored water is injected through the SEN for a time period of 1.5 s into the mold.
In the same way numerical ink experiments with the species transport model and the corresponding boundary conditions have been carried out for the standard bifurcated SEN (Fig. 4).

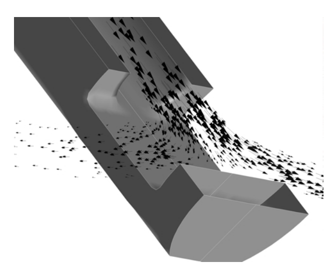

**Figure 4:** Standard bifurcated SEN

Water model experiments which identify three completely different mold flow patterns were reproduced with numerical simulations.

#### *Single roll flow pattern*

For a slab mold width of 2 m, a submergence depth of 100 mm and a casting speed of 1 m/min the standard SEN produces a so called single roll flow pattern (Gotthelf et al., 1998). The result of the numerical ink experiment (Fig. 5 - left side) and the corresponding snap shot of a video clip (Fig. 5 – right side) show the propagation of the ink cloud. Colored fluid leaves the SEN side ports and moves directly towards the free surface. Fig. 5 shows an unusual large circulation which moves from the side port outlets to the meniscus and down along the narrow mold side.

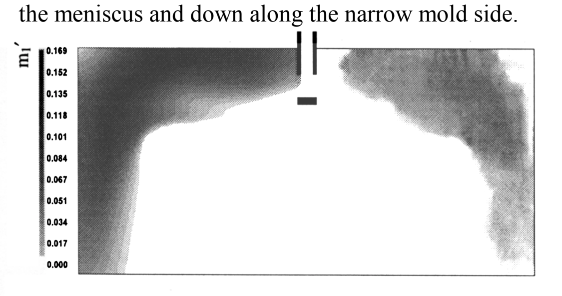


**Figure 5:** Mass fraction of colored fluid $m_l'$ (left), snap shot of water trial (right) for a single roll flow pattern

The Coanda effect (Schlichting and Gersten, 1997), which describes the behavior of a jet which is injected near a wall attaching to that wall after a certain distance, seems to play an important role in this case.

***Double roll flow pattern***

The same configuration was tested for a casting speed of 1.4 m/min. As shown in Fig. 6 the ink cloud moves towards the narrow side of the mold without touching the top surface of the liquid pool and is splitted at the impingement point at the narrow into an upper and a lower recirculation (Gotthelf et al., 1998).

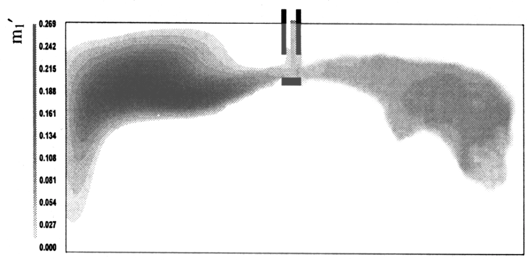


**Figure 6:** Mass fraction of colored fluid $m_l'$ (left), snap shot of water trial (right) for a double roll flow pattern

For slab width variations a similar change in the flow patterns was also detected in experimental and numerical studies. Unsteady flow pattern could not be observed in water model trails used to validate the calculated results in this paper (injection time of 1.5 s of colored fluid was too short) but have been reported by Honeyands et al. (1992) and Gebhard et al. (1993).

**Advanced nozzle design**

***Stabilization of the mold flow with an additional SEN base hole***

Typical flow pattern at the side port outlets for the standard bifurcated SEN are shown at the wide symmetry plane in Fig. 7. Recirculation zones below the upper edge of the side port can be detected which initialize disturbances leading to a destabilization of the side port jets.

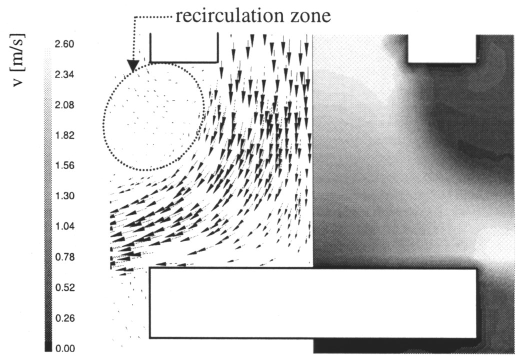


**Figure 7:** Velocity vectors and contours colored by velocity magnitude for the standard bifurcated SEN

Numerical simulations of mold flows with the standard SEN at a mold width of 2.5 m, a submergence depth of 150 mm and a casting speed of 1m/min predict oscillating flow pattern with a time period of 28 s (Fig. 8). These oscillations are characterized by a fluctuating side jet inducing an impingement point position which moves from the meniscus to the narrow mold side and vice versa.

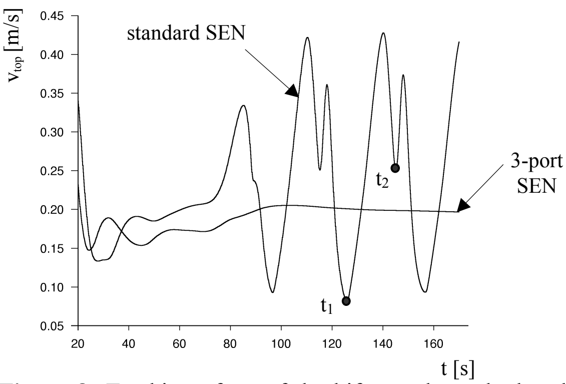


**Figure 8:** Tracking of $v_{top}$ of the bifurcated standard and modified 3-port SEN

Contour plots of velocity magnitude in the symmetry plane of the half slab width with the corresponding maximum wave height $\Delta h_{max}$ and $T_{top}$ at different simulation times $t_1$ and $t_2$ (Fig. 8) are documented in the following figures (Fig. 9a and Fig. 9b).

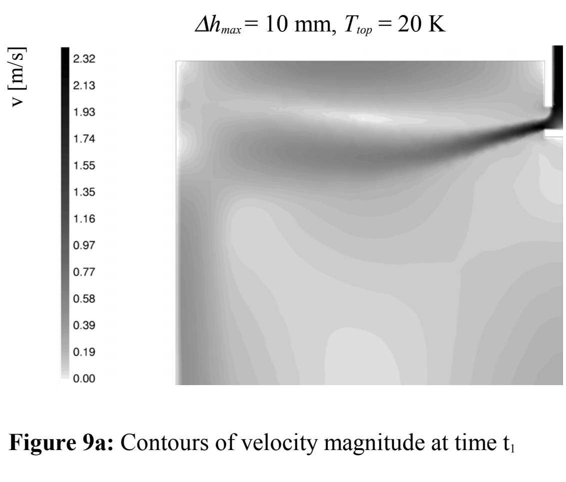


**Figure 9a:** Contours of velocity magnitude at time $t_1$

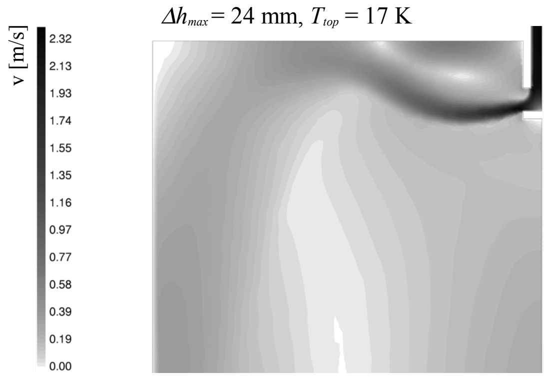


**Figure 9b:** Contours of velocity magnitude at time $t_2$

To stabilize the unsteady mold flow an additional small hole was placed in the base center (Fig. 10) of the standard bifurcated nozzle (Fig. 4).

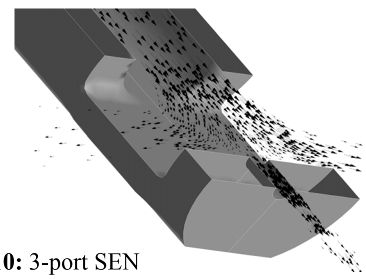

**Figure 10:** 3-port SEN

The resulting quasi-steady behavior of mold flow induced by the modified SEN (Fig. 10) shows a nearly constant $v_{top}$ of 0.18 m/s for simulation times higher than 110 s (Fig. 8). Oscillating flow structures were replaced by a single roll structure similar to Fig. 9b.

Wave heights up to 18 mm may lead to slag entrapment which apparently reduce the cast steel quality products (Gotthelf et al., 1998; Heaslip and Schade, 1999). Calculated wave heights scaled with $\Delta h_{max}$ and $T_{ab}$ scaled with $T_{ab,max}$ at the meniscus which are induced by the modified SEN geometry are shown in Fig. 11.

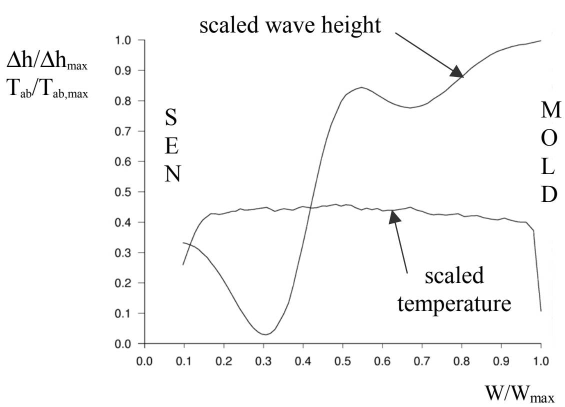


**Figure 11:** $\Delta h/\Delta h_{max}$, $T_{ab}/T_{ab,max}$ at the wide symmetry plane: 3-port SEN

The side port jets move directly toward the top surface and generate a so called hot spot at the position of the impingement point. However, more mold powder will be molten in this region than in other regions of the meniscus and a break up of the powder layer cannot be excluded. The temperature above liquidus temperature ($T_{ab}$) in the symmetry plane of the half slab width is detailed in Fig. 12.

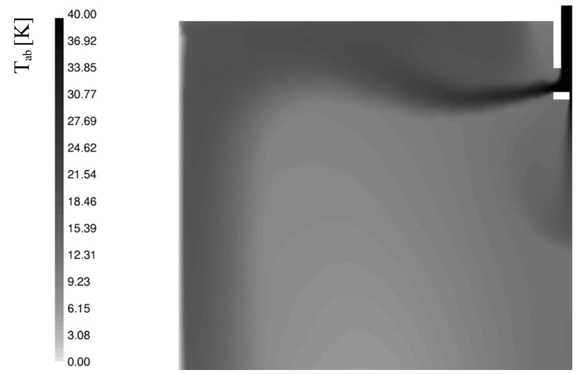


**Figure 12:** Contours of $T_{ab}$: 3-port SEN

Simulation results for the stabilizing 3-port nozzle for slab width up to 3 m are quite similar to those of slab width 2.5 m.

***Optimized bifurcated SEN inducing quasi-steady double roll flow pattern***

Various CFD calculations with different SEN geometries and operating conditions were carried out resulting in a bifurcated nozzle design with the desired mold flow characteristics.

The previous CFD simulations described the stabilization effect of an additional base hole with non satisfying single roll flow patterns at enormous wave heights. An improvement of the side port flow condition could be attained by eliminating the recirculation zones near these ports (Fig. 13).

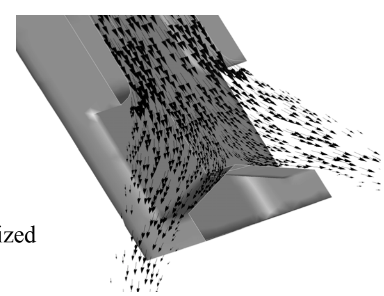

**Figure 13:** Optimized bifurcated SEN

For a mold slab width of 3 m, a submergence depth of 225 mm and a casting speed of 1 m/min the unsteady calculation procedure, leading to quasi-steady steel flow, can be tracked in Fig. 14.

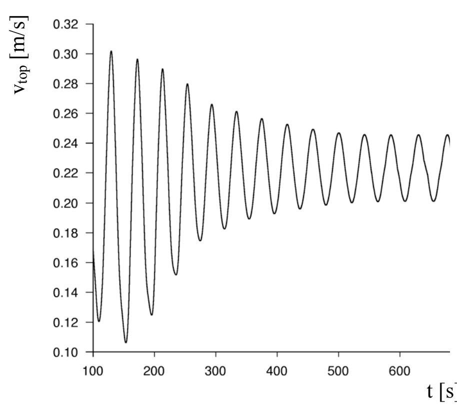


**Figure 14:** Tracking of $v_{top}$ with the simulation time for the optimized bifurcated SEN

Contours of velocity magnitudes (Fig. 15) show a quasi-steady side port jet moving towards the narrow side of the mold and generating double roll flow patterns with a large upper recirculation.

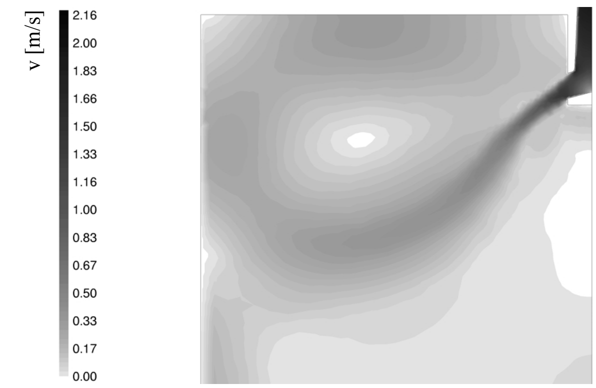


**Figure 15:** Contours of velocity magnitude: Optimized bifurcated SEN

The calculated scaled wave height and scaled temperature above $T_{liq}$ are detailed in Fig. 16. To make clear the differences between the results of 3-port and bifurcated SEN the same scaling parameters as in Fig. 11 were used.

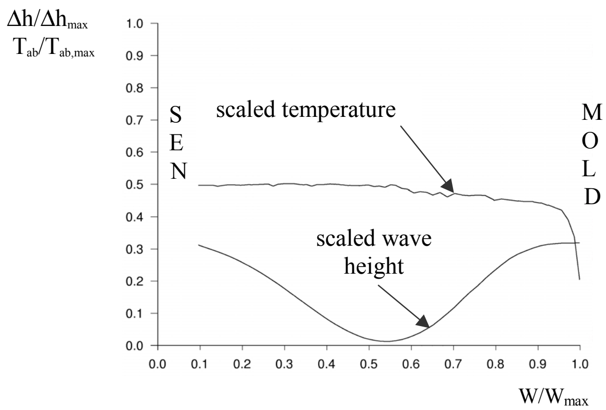


**Figure 16:** $\Delta h/\Delta h_{max}$, $T_{ab}/T_{ab,max}$ at the wide symmetry plane: Optimized bifurcated SEN

A higher and more homogenous temperature distribution at the meniscus (Fig. 16, Fig. 17) and a reduction of the maximum wave height to approximately one third of the calculated $\Delta h_{max}$ of the 3-port SEN (Fig. 16) seem to be good operating conditions for high quality slabs.

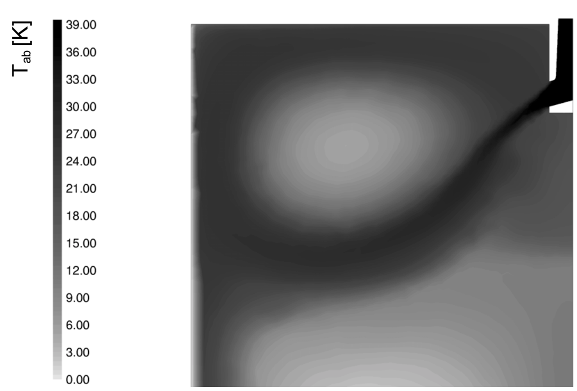


**Figure 17:** Contours of $T_{ab}$: Optimized bifurcated SEN

Similar quasi-steady flow and temperature fields have been calculated for the optimized SEN at a mold slab width of 2.5 m, a submergence depth of 225 mm and a casting speed of 1 to 1.25 m/min.

## CONCLUSION

The presented report shows that CFD tools can be efficiently used to understand and optimize the unsteady turbulent flow behavior in the mold region of wide slab casters. A series of numerical calculations led to an improved SEN design which induces a quasi-steady double roll flow field with an impingement point at the narrow side of the slab mold at moderate wave heights for slab widths up to 3 m. Temperature calculations show a homogenous and sufficient high temperature distribution at the top of the liquid steel pool. The investigated bifurcated SEN for wide slab casters is successfully used and first casting results confirm the simulation results of the numerical studies presented here.

## REFERENCES

FLUENT INC., (1998), "User's Guide for FLUENT 5", Lebanon, USA.

GEBHARD, M., He, Q.L. and HERBERTSON, J., (1993), "Vortexing Phenomena in Continuous Slab Casting Molds", *Steel making Conference Proceedings*, Vol. 76, Dallas, Texas.

GOTTHELF, D., ANDRZEJEWSKI, P., JULIUS, E., HAUBRICH, H., (1998), "Mould Flow Monitoring – A Tool to improve Caster Operation", *3rd European Conference on Continuous Casting,* Madrid, Spain.

HEASLIP, L. J. and SCHADE, J., (1999) "Physical Modelling and Visualization of Liquid Steel Flow behavior during Continuous Casting", *ISS Alex McLean Symposium*, Toronto, Ontario, Canada.

HONEYANDS, T.A., LUCAS, J. and CHAMBERS, J., (1992), "Modelling of Steel Delivery and Fluid Flow in Thin Slab Caster Moulds", *11th Australasian Fluid Mechanics Conference,* Hobart, Australia.

HONEYANDS, T.A. and HERBERTSON, J., (1994), "Oscillations in Thin Slab Caster Mold Flows", *127th ISIJ Meeting*, Tokyo, Japan.

LAUNDER, B. A. and SPALDING, D.B., (1972), "Lectures in Mathematical Models of Turbulence", *Academic Press*, London, England.

LAUNDER, B. A. and SPALDING, D.B., (1974), "The Numerical Computation of Turbulent Flows", *Computer Methods in Applied Mechanics and Engineering*, 3: 269-289.

SCHLICHTING, H. and GERSTEN, K., (1997) "Grenzschicht-Theorie", *Springer-Verlag*, Germany.

YAKHOT, V. and ORSZAG, S. A., (1992), "Renormalization Group Analysis of Turbulence. I. Basic Theory", *J. of Science Computing*, Vol. 1, No. 1, 1-151.